laterality index (LI) was calculated for each subject as a measure of the laterality of neural processes [14]. The LI of each subject was based on the proportion of activated voxels (uncorrected $P < 0.05$ and 50 contiguous voxels) in the left (L) and right (R) parietal regions, as defined by the Anatomical Automatic Labeling atlas [17]. The LI was calculated according to the following formula: $LI = (L - R)/(L + R)$. Previous studies have reported that LI represents hemispheric predominance: $-1 < LI < -0.25$ indicates right-side dominance; $-0.25 < LI < 0.25$ indicates bilateral activation; and $0.25 < LI < 1$ indicates left-side dominance [14]. We classed subjects as 'left-hemisphere dominance', 'bilateral activation', or 'right-hemisphere dominance', according to these boundaries. According to these criteria, nine subjects showed left-hemisphere dominance (four females; mean age, 20.8 years; range, 20–23 years, LI, 0.61 ± 0.23). The other seven subjects showed bilateral activation (one female; mean age, 21.4 years; range, 20–23 years, LI, 0.01 ± 0.15). No subjects showed right-hemisphere dominance. There was no difference in age ($t = 1.10$, $P = 0.290$) or sex ($\chi^2 = 1.667$, $P = 0.197$) between these groups. Although the number of subjects in each group was not identical (left-hemisphere dominance $n = 9$, bilateral activation $n = 7$), there was no difference in the variance of response time in the tDCS experiment between these groups (Levine's test for equality of variance, $P = 0.335$).

2.3. tDCS experiment

The subjects participated in three tDCS sessions, each performed 1 week apart. In one tDCS session, anodal tDCS was applied over the left parietal cortex and cathodal tDCS was applied over the right parietal cortex (LARC). In another session, cathodal tDCS was applied over the left parietal cortex and anodal tDCS was applied over the right parietal cortex (LCRA). In the third session, sham tDCS was applied over both parietal cortices.

2.3.1. tDCS mental calculation task

In each tDCS session, subjects performed a mental calculation task at four time points: pre-, during-, 30 min post-, and 60 min post-tDCS (Fig. 1B). As a control, subjects performed a choice reaction task immediately after the calculation task at each of the four time points.

During the tDCS experiment, subjects sat in a chair in front of a computer screen. A multiplication problem comprising a two-digit number and a one-digit number was presented on the screen for 8 s as "Problem". Instead of selecting the correct answer from choices, the subjects were required to type the answer on a numeric keypad as quickly as possible (Fig. 1A, right). For example, if "64 × 7" was presented as "Problem", the subject was required to push "4", "4", and "8" on the keypad. Thus, the method by which a response was made to the calculation task differed between fMRI and tDCS experiments. In the choice reaction task, the subjects were presented with the same set of "Problems" but were not required to perform a multiplication calculation. They were instead required to push buttons on the numeric keypad that corresponded to the numbers presented. For example, if "64 × 7" was presented, the subject was required to push "6", "4", and "7" on the keypad.

Performance was quantified by response time, defined as the time from the appearance of the "Problem" until the last button was pressed in the answer, and accuracy of forty-two trials was performed at each time point.

2.3.2. tDCS procedure

A DC Stimulator Plus (NeuroConn, Ilmenau, Germany) delivered direct current through two sponge surface electrodes, each with a surface area of 35 cm^2, that were soaked in 15 mM NaCl [5]. The electrodes were placed bilaterally on the scalp, over the parietal region. For each subject, the centers of the stimulation electrodes were placed over the area of the parietal lobe that was identified in the fMRI experiment as showing the peak parietal voxel in non-normalized anatomical space. The peak voxel of the left and right partial cortex was identified independently. This area was located using a frameless stereotaxic navigation system (Brainsight, Rogue Research Inc., Montreal, Canada). tDCS was applied for 10 min. The current density at the electrodes was 0.057 mA/cm^2, and the total charge was 0.069 C/cm^2. These parameters are far below the thresholds for tissue damage [11]. The stimulation started 3 min before the 'during-tDCS' calculation task was performed. For sham stimulation, the same procedure was used but current was applied for only the initial 30 s of the 10 min 'stimulation period' [7].

2.3.3. tDCS data analysis

The average response time and accuracy for each task (calculation task; choice reaction task) was calculated at each time point (pre-, during-, 30 min post-, and 60 min post-tDCS) for each subject. There were no significant differences at the pre-tDCS time points between the conditions (calculation task; $F_{(2, 45)} = 0.107$, $P = 0.899$, control task; $F_{(2, 45)} = 0.174$, $P = 0.841$). Thus, we normalized the response time and accuracy at the during-, 30 min post-, and 60 min post-tDCS time points to the response time at the pre-tDCS time point. Normalized response times and accuracies are presented in the results section. Raw response times and accuracies are presented in Supplementary Data. The normalized response times and accuracies were subjected to a three-way repeated measures analysis of variance (ANOVA) of tDCS session (LARC; LCRA; sham), task (calculation task; choice reaction task), and time point (during; 30 min post; 60 min post). This ANOVA was performed separately for each group of subjects (left-hemisphere dominant; bilateral activation). Post hoc tests with Bonferroni corrections were performed where appropriate.

3. Results

3.1. fMRI experiment

The group-level analysis revealed higher parietal activation during the task blocks than during the rest blocks. The peak coordinate of the parietal activity was observed in the intraparietal sulcus (peak MNI coordinate of the left hemisphere, $x = -34$, $y = -50$, $z = 48$; $t = 8.69$; peak MNI coordinate of the right hemisphere, $x = 38$, $y = -44$, $z = 40$; $t = 7.49$). Nine of the 16 subjects showed left-hemisphere dominance, and the other seven subjects showed bilateral activation. No subjects showed right-hemisphere dominance. These findings compare well with those of previous fMRI studies [4].

3.2. tDCS experiment

There was no significant difference in performance (response time and accuracy) between subjects with left-hemisphere dominance ($n = 9$) and subjects with bilateral activation ($n = 7$) at the pre-tDCS time point in either the calculation task (response time $P = 0.110$, accuracy $P = 0.838$) or the choice reaction task (response time $P = 0.985$, accuracy $P = 0.404$).

3.2.1. Response time in subjects with left-hemisphere dominance ($n = 9$)

For normalized response time, there was a significant interaction between tDCS session and task ($F_{(2,16)} = 8.081$, $P = 0.004$), but no other significant main effects or interactions ($P > 0.13$). The interaction between tDCS session and task indicates that the effects of tDCS on normalized response time were different between the calculation task and the choice reaction task, but there was no influence of time point (during-, 30 min post-, and 60 min post-tDCS)

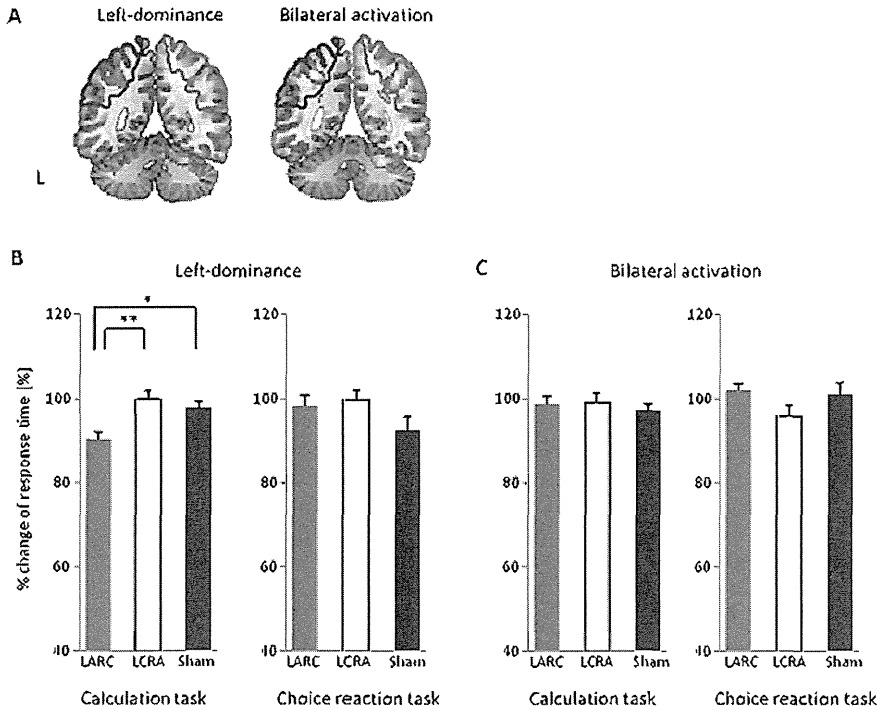

Fig. 2. (A) Parietal activity during the calculation block relative to the rest block for the subjects with left-hemispheric dominance (left panel) and the subjects with bilateral activation (right panel). The voxel-wise threshold was set at $P<0.005$ uncorrected at the voxel level, followed by family-wise error correction for multiple comparisons at the cluster level at $P<0.05$. The regions of interest are indicated by red (L: left parietal cortex) and blue (R: right parietal cortex) lines [17]. (B and C) The results of tDCS experiment. Normalized Response time in the calculation and the choice reaction tasks in (B) subjects with left-hemisphere dominance (B) and (C) subjects with bilateral activation. tDCS was applied with the anode over the left parietal cortex and the cathode over the right parietal cortex (LARC, gray), with the cathode over the left parietal cortex and the anode over the right parietal cortex (LCRA, white) and in a sham form (sham, black). Error bars indicate the standard error of the mean. $^{*}P<0.05$; $^{**}P<0.01$.

in each task. To investigate this further, the normalized response time was averaged across all three time points, and the effect of tDCS was investigated separately for each task using a one-way repeated measures ANOVA. In the calculation task, there was a significant main effect of tDCS session on normalized response time ($F_{(2,26)}=6.60$, $P=0.005$, Fig. 2B left). The normalized response time was shorter in the LARC tDCS session ($90.2\pm1.88\%$) than in the sham ($97.8\pm1.65\%$, $P=0.036$) and LCRA ($99.8\pm2.33\%$, $P=0.006$) tDCS sessions. The normalized response time in the LCRA tDCS session was not different from that in the sham tDCS session ($P=1.000$). By contrast, there was no significant main effect of tDCS session on normalized response time in the choice reaction task ($F_{(2,26)}=0.16$, $P=0.86$, Fig. 2B right).

3.2.2. Response time in subjects with bilateral activation (n = 7)

For normalized response time, there was a significant main effect of time point ($F_{(2,12)}=7.220$, $P=0.009$), but no other significant main effects or interactions ($P>0.05$, Fig. 2C). This indicates that there was no significant effect of tDCS on normalized response time in subjects with bilateral activation.

3.2.3. Group comparison of response time

A direct group comparison of normalized response time (averaged over all three time points) between subjects with left-hemisphere dominance and subjects with bilateral activation revealed that average normalized response time in the LARC tDCS session was shorter in subjects with left-hemispheric dominance ($90.2\pm1.88\%$) than in subjects with bilateral activation ($98.2\pm2.56\%$; two-sample t-test, $t=2.58$, $P=0.022$).

3.2.4. Accuracy

For normalized accuracy, there were no significant main effects or interactions ($P>0.05$) for either subject group. This indicates that there was no significant effect of tDCS on normalized accuracy. We used a questionnaire to ask subjects for their discomfort and fatigue after tDCS. However, there was no difference in these factors between tDCS conditions.

4. Discussion

In the present study, we examined whether the effect of bilateral parietal tDCS differed among individuals according to the functional lateralization of brain activity observed during a mental calculation task. In subjects with a parietal LI that indicated left-hemisphere dominance, response time was significantly shortened when anodal tDCS was applied over the left parietal cortex and cathodal tDCS was applied over the right parietal cortex. This facilitative effect was not observed in subjects without left-hemispheric dominance of parietal activity. These results indicate that the facilitative effect of LARC bilateral tDCS over the parietal cortex was specific to subjects with left-hemispheric dominance in the parietal cortex. In these subjects, LARC tDCS may have enhanced the existing lateralization to induce an improvement in response time. By contrast, the lateralization induced by LARC tDCS may not be beneficial to subjects in whom the intrinsic pattern of activity was balanced between the two hemispheres.

In subjects with left-hemisphere dominance, LARC tDCS affected response time, whereas LCRA tDCS and sham tDCS did not. This could be due to a combined effect of increased excitability in the left parietal cortex, where the neural basis of multiplication is localized [4], and decreased inter-hemispheric inhibition from the right to the left parietal cortex, probably via inter-hemispheric connections, during LARC tDCS. Inter-hemispheric inhibition has long been recognized as a concept of "rivalry" between the two hemispheres, and motor function in the cortex of one hemisphere is promoted

by inhibitory transcranial magnetic stimulation of the contralateral cortex [19].

Similarly, we expected that LCRA tDCS would inhibit performance of the calculation task. However, LCRA tDCS did not affect response time in the calculation task. The reason for this negative result is unclear. One possibility is that subjects might have changed the strategy that they used to perform mental calculations during LCRA tDCS so that they were not disrupted by the inhibition of left parietal activity by cathodal tDCS. It has been reported that humans can use a different strategy for mental calculation that primarily relies on the premotor and superior parietal regions [8]. Future study should investigate the relation between the strategy used for mental calculation and effect of brain stimulation on the performance of mental calculations.

Importantly, in subjects with left-hemisphere dominance we observed LARC tDCS-induced changes in response times in the calculation task but not the choice reaction task. The choice reaction task consisted of number perception, decision-making, stimulus-response association, and finger movement. The lack of a tDCS-induced effect in the choice reaction task indicates that the change in response time in the calculation task was not due to an influence of tDCS on any of these non-specific factors, and supports the concept that tDCS influenced the performance of mental calculation.

Recent studies have demonstrated that anodal or cathodal stimulation over the right parietal cortex can affect performance of a spatial attention task [1,18]. Therefore, the present result may be explained by a facilitative effect of right parietal cortex stimulation on attentional function. However, in subjects with left-hemisphere dominance, fMRI activation in the right parietal cortex was smaller than in the left parietal cortex, indicating that spatial attentional function of the right parietal cortex might be less relevant cognitive process for these subjects. Therefore, we believe that the effect of tDCS on spatial attention is minimal in the present study.

We cannot exclude the possibility that the mental calculation process studied here involves a process similar to the manipulation of working memory content (so-called 'central executive') in addition to the access to the arithmetic table. We consider the interaction between the arithmetic table and central executive to be the core process involved in mental calculations, and these processes cannot be separated using the current data. Therefore, our results represent the effect of tDCS on both of these processes woven together. In future, we should ask whether the effect of tDCS is specific to one of the two cognitive processes or an interaction of the two processes.

In the present study, we used only bilateral tDCS. Thus, we cannot rule out the possibility that unilateral parietal tDCS might have been sufficient to evoke changes in behavioral performance. In a preliminary experiment with six healthy subjects, we investigated the effect of unilateral parietal tDCS (one electrode over the left or right parietal cortex, reference electrode over the chin) on response times in the same calculation task, but we did not observe any tendency toward changes in response times. Therefore, it is reasonable to consider that bilateral stimulation is necessary to induce the behavioral changes observed in the present study. Nonetheless, future studies should clarify this issue by investigating unilateral stimulation-induced effects on behavior. In the present study, we found a significant effect of tDCS only on response times that had been normalized to the pre-tDCS value, and not on raw response times. This might be due to the small number of subjects and is a limitation of the present study. Future studies with larger sample size should clarify this point.

In conclusion, bilateral tDCS with the anode over the left parietal cortex and the cathode over the right parietal cortex enhanced the performance of mental calculation in subjects with left-hemisphere dominance of activity during mental calculations. This indicates that fMRI may be useful for predicting individuals who would benefit from bilateral tDCS.

Acknowledgments

This research was supported by funding from the JPSS KAKENHI for Manabu Honda (22240049), Satoshi Tanaka (24680061) and MEXT KAKENHI for Manabu Honda (22135008).

Appendix A. Supplementary data

Supplementary data associated with this article can be found, in the online version, at http://dx.doi.org/10.1016/j.neulet.2013.04.022.

References

[1] N. Bolognini, E. Olgiati, A. Rossetti, A. Maravita, Enhancing multisensory spatial orienting by brain polarization of the parietal cortex, Eur. J. Neurosci. 31 (2010) 1800–1805.
[2] C. Calautti, M. Naccarato, P.S. Jones, N. Sharma, D.D. Day, A.T. Carpenter, E.T. Bullmore, E.A. Warburton, J.C. Baron, The relationship between motor deficit and hemisphere activation balance after stroke: a 3T fMRI study, Neuroimage 34 (2007) 322–331.
[3] R. Cohen Kadosh, S. Soskic, T. Iuculano, R. Kanai, V. Walsh, Modulating neuronal activity produces specific and long-lasting changes in numerical competence, Curr. Biol. 20 (2010) 2016–2020.
[4] S. Dehaene, N. Molko, L. Cohen, A.J. Wilson, Arithmetic and the brain, Curr. Opin. Neurobiol. 14 (2004) 218–224.
[5] J.E. Dundas, G.W. Thickbroom, F.L. Mastaglia, Perception of comfort during transcranial DC stimulation: effect of NaCl solution concentration applied to sponge electrodes, Clin. Neurophysiol. 118 (2007) 1166–1170.
[6] R. Everts, K. Lidzba, M. Wilke, C. Kiefer, M. Mordasini, G. Schroth, W. Perrig, M. Steinlin, Strengthening of laterality of verbal and visuospatial functions during childhood and adolescence, Hum. Brain Mapp. 30 (2009) 473–483.
[7] P.C. Gandiga, F.C. Hummel, L.G. Cohen, Transcranial DC stimulation (tDCS): a tool for double-blind sham-controlled clinical studies in brain stimulation, Clin. Neurophysiol. 117 (2006) 845–850.
[8] T. Hanakawa, M. Honda, T. Okada, H. Fukuyama, H. Shibasaki, Neural correlates underlying mental calculation in abacus experts: a functional magnetic resonance imaging study, Neuroimage 19 (2003) 296–307.
[9] L. Jacobson, M. Koslowsky, M. Lavidor, tDCS polarity effects in motor and cognitive domains: a meta-analytical review, Exp. Brain Res. 216 (2012) 1–10.
[10] K.T. Jones, M.E. Berryhill, Parietal contributions to visual working memory depend on task difficulty, Front. Psychiatry 3 (2012) 81.
[11] M.A. Nitsche, D. Liebetanz, N. Lang, A. Antal, F. Tergau, W. Paulus, Safety criteria for transcranial direct current stimulation (tDCS) in humans, Clin. Neurophysiol. 114 (2003) 2220–2222, author reply 2222–2223.
[12] M.A. Nitsche, W. Paulus, Excitability changes induced in the human motor cortex by weak transcranial direct current stimulation, J. Physiol. 527 (Pt 3) (2000) 633–639.
[13] M.C. Ridding, U. Ziemann, Determinants of the induction of cortical plasticity by non-invasive brain stimulation in healthy subjects, J. Physiol. 588 (2010) 2291–2304.
[14] M.L. Seghier, Laterality index in functional MRI: methodological issues, Magn. Reson. Imaging 26 (2008) 594–601.
[15] S. Tanaka, M. Sandrini, L.G. Cohen, Modulation of motor learning and memory formation by non-invasive cortical stimulation of the primary motor cortex, Neuropsychol. Rehabil. 21 (2011) 650–675.
[16] P. Tseng, T.Y. Hsu, C.F. Chang, O.J. Tzeng, D.L. Hung, N.G. Muggleton, V. Walsh, W.K. Liang, S.K. Cheng, C.H. Juan, Unleashing potential: transcranial direct current stimulation over the right posterior parietal cortex improves change detection in low-performing individuals, J. Neurosci. 32 (2012) 10554–10561.
[17] N. Tzourio-Mazoyer, B. Landeau, D. Papathanassiou, F. Crivello, O. Etard, N. Delcroix, B. Mazoyer, M. Joliot, Automated anatomical labeling of activations in SPM using a macroscopic anatomical parcellation of the MNI MRI single-subject brain, Neuroimage 15 (2002) 273–289.
[18] M. Weiss, M. Lavidor, When less is more: evidence for a facilitative cathodal tDCS effect in attentional abilities, J. Cogn. Neurosci. 24 (2012) 1826–1833.
[19] J.A. Williams, A. Pascual-Leone, F. Fregni, Interhemispheric modulation induced by cortical stimulation and motor training, Phys. Ther. 90 (2010) 398–410.

frontiers in
SYSTEMS NEUROSCIENCE

ORIGINAL RESEARCH ARTICLE
published: 11 April 2013
doi: 10.3389/fnsys.2013.00006

Transcranial direct-current stimulation increases extracellular dopamine levels in the rat striatum

*Tomoko Tanaka[1], Yuji Takano[2,3], Satoshi Tanaka[4], Naoyuki Hironaka[2,3], Kazuto Kobayashi[5], Takashi Hanakawa[1,6], Katsumi Watanabe[7] and Manabu Honda[1,6]**

[1] Department of Functional Brain Research, National Institute of Neuroscience, National Center of Neurology and Psychiatry, Tokyo, Japan
[2] Human Information Science Laboratory, NTT Communication Science Laboratories, Kanagawa, Japan
[3] CREST, Japan Science and Technology Agency, Saitama, Japan
[4] Center for Fostering Young and Innovative Researchers, Nagoya Institute of Technology, Aichi, Japan
[5] Department of Molecular Genetics, Institute of Biomedical Science, Fukushima Medical University School of Medicine, Fukushima, Japan
[6] Integrative Brain Imaging Center, National Center of Neurology and Psychiatry, Tokyo, Japan
[7] Cognitive Science Laboratory, University of Tokyo, Tokyo, Japan

Edited by:
Detlef H. Heck, University of Tennessee Health Science Center, USA

Reviewed by:
Alessandro Stefani, University of Rome, Italy
Masahiko Takada, Kyoto University, Japan

***Correspondence:**
Manabu Honda, Department of Functional Brain Research, National Institute of Neuroscience, National Center of Neurology and Psychiatry, 4-1-1 Ogawa-Higashi, Kodaira, Tokyo 187-8502, Japan
e-mail: honda@ncnp.go.jp

Background: Transcranial direct-current stimulation (tDCS) is a non-invasive procedure that achieves polarity-dependent modulation of neuronal membrane potentials. It has recently been used as a functional intervention technique for the treatment of psychiatric and neurological diseases; however, its neuronal mechanisms have not been fully investigated *in vivo*.

Objective/Hypothesis: To investigate whether the application of cathodal or anodal tDCS affects extracellular dopamine and serotonin levels in the rat striatum.

Methods: Stimulation and *in vivo* microdialysis were carried out under urethane anesthesia, and microdialysis probes were slowly inserted into the striatum. After the collection of baseline fractions in the rat striatum, cathodal or anodal tDCS was applied continuously for 10 min with a current intensity of 800 μA from an electrode placed on the skin of the scalp. Dialysis samples were collected every 10 min until at least 400 min after the onset of stimulation.

Results: Following the application of cathodal, but not anodal, tDCS for 10 min, extracellular dopamine levels increased for more than 400 min in the striatum. There were no significant changes in extracellular serotonin levels.

Conclusion: These findings suggest that tDCS has a direct and/or indirect effect on the dopaminergic system in the rat basal ganglia.

Keywords: basal ganglia, dopamine, Parkinson disease, transcranial direct current stimulation, striatum

INTRODUCTION

Transcranial direct-current stimulation (tDCS) is a non-invasive technique in which a weak DC is used to polarize target brain regions (Nitsche and Paulus, 2000). Several studies have previously shown that tDCS affects motor function and learning in healthy subjects, presumably by changing the neuronal activity of the stimulated site (Wassermann and Grafman, 2005; Tanaka et al., 2009; Bachmann et al., 2010; Fox, 2011; Schambra et al., 2011). It is also effective in patients with psychiatric and neurological diseases, and so has the potential to be used as an adjuvant strategy in the rehabilitation of motor and cognitive deficits caused by neurological disorders (Hummel et al., 2005; Boggio et al., 2006; Fregni et al., 2006; Lefaucheur, 2009; Murphy et al., 2009; Nitsche et al., 2009; Benninger et al., 2010; Tanaka et al., 2011a; Brunoni et al., 2012). In addition, some *in vivo* animal studies have investigated the behavioral and biological effects of tDCS (Kim et al., 2010; Wachter et al., 2011; Laste et al., 2012). Nevertheless, the mechanisms underlying tDCS are largely unknown, particularly with regard to its effects on the neuronal network.

tDCS directly modulates neuronal membrane potentials beneath the stimulus electrode. However, it might also have a remote or systematic effect on the neuronal circuit. Indeed, increasing evidence from human electrophysiological and neuroimaging studies suggests that tDCS modulates brain activities in cortical or subcortical areas other than the stimulated site (Lang et al., 2005; Bachmann et al., 2010; Antal et al., 2011; Binkofski et al., 2011; Halko et al., 2011), possibly via anatomical connections (Veening et al., 1980; Selemon and Goldman-Rakic, 1985; McGeorge and Faull, 1989). Recently, human experiments using fMRI reported that tDCS can also modulate resting-state functional connectivity in distinct functional networks of the brain (Keeser et al., 2011). Furthermore, it has been demonstrated that an increase of phosphorylation of trkB, which is a receptor of Brain-derived neurotrophic factor (BDNF), was induced by DCS *in vitro* (Fritsch et al., 2010). These comprehensive

effects through neuronal networks may be observable at the neurotransmitter level, as well as at the electrophysiological and metabolic levels. Previously, pharmacological approaches based on human drug intake have suggested the involvement of glutamatergic, γ-aminobutyric acid (GABA)-ergic, and dopaminergic systems in long-term tDCS effects (Liebetanz et al., 2002; Nitsche et al., 2003). These experiments, however, reported modulation of tDCS effects by neurotransmitter operations, and used motor-evoked potentials (MEPs) as outcome measurements. Consequently, they provided indirect measurements of neurotransmitters, which inherently limited the interpretation of results. In the present study, being an important factor in the introduction of a remote network effect, we focused on the change in neurotransmitter levels.

The present study directly measured changes in the extracellular dopamine level in the basal ganglia induced by tDCS using *in vivo* microdialysis in a rat model. This invasive procedure directly and locally measures compounds, such as extracellular dopamine, via a probe inserted into a target brain region (Navailles et al., 2004; Nitsche et al., 2006). Dopamine transmission in the striatum plays an essential role in the modulation of motor and cognitive symptoms caused by neurological disorders such as Parkinson's disease (PD) (Carlsson, 1972; Fahn, 2003), as well as in learning-induced neuroplasticity in both humans and rats (Adcock et al., 2006; Berridge, 2007; Rossato et al., 2009; Tanaka et al., 2011b). To understand the underlying mechanism of tDCS behavioral effects, we examined whether its application affected the dopaminergic systems in the striatum and showed that it had a direct and/or indirect effect.

MATERIALS AND METHODS

The experimental protocol was approved by the Animal Care and Use Committee of the National Institute of Neuroscience (National Center of Neurology and Psychiatry, Tokyo, Japan). The experiments were conducted in accordance with the "Official Notification on Animal Experiments" (National Institute of Neuroscience, National Center of Neurology and Psychiatry notification no. 2010004, received 2010). Every effort was made to minimize the number of animals used in the experiments and their suffering.

ANIMALS

Male nine-week old Sprague Dawley rats (CLEA Japan, Inc., Tokyo, Japan) were housed at a temperature of 23 ± 1°C with a 12-h light/dark cycle (lights-on 08:00–20:00). Food and water were available *ad libitum*. Twenty-five rats were used for the microdialysis experiment, and 12 were used to investigate tissue damage.

MICRODIALYSIS SURGERY

Twenty-five rats were divided into the following three groups: cathodal tDCS ($n = 7$), anodal ($n = 7$), and sham ($n = 7$). After at least 3 days of habituation to the animal colony, all rats were intraperitoneally (i.p.) anesthetized with a single shot of urethane (1 g/kg body weight) and placed in a stereotaxic apparatus. The skull was exposed and a small hole was made using a dental drill. A guide cannula (AG-6; Eicom Corporation, Kyoto, Japan) was implanted into the striatum [+1.0 mm anterior, +3.5 mm lateral, and −4.5 mm ventral to the bregma according to the stereotaxic atlas of Paxinos and Watson (1998)]. The guide cannula was fixed to the skull with resin dental cement.

tDCS

The experimental tDCS setup was similar to that reported by Takano et al. (2010). One electrode of the stimulator (5 mm × 5 mm size) was fixed with surgical tape on the skin above the brain region including the cortex, and positioned in reference to the insertion point of the microdialysis guide cannula (Figure 1A) at an anatomical location roughly corresponding to +2.0 to +7.0 mm anterior and +1.0 to +6.0 mm lateral to the bregma (Paxinos and Watson, 1998). It was previously reported that the frontal cortex beneath the stimulation electrode had an anatomical connection to the striatum where the microdialysis probe was implanted (Ebrahimi et al., 1992; Gabbott et al., 2005). A second electrode was placed on the animal's neck in a similar way.

Cathodal or anodal tDCS was applied continuously for 10 min with a current intensity of 800 μA from the scalp electrode using a DC stimulator (STG1002; Multi Channel Systems, Germany). Cathodal stimulation was applied for 10 s to the sham group with a current intensity of 10 μA from the scalp electrode. The safety limit of the stimulator was 120 V. The current intensity of 800 μA, corresponding to a current density of 32.0 A/m^2 in the present setting, was used to maximize the effects of tDCS within the safety limits reported in a previous rat tDCS study using cathodal

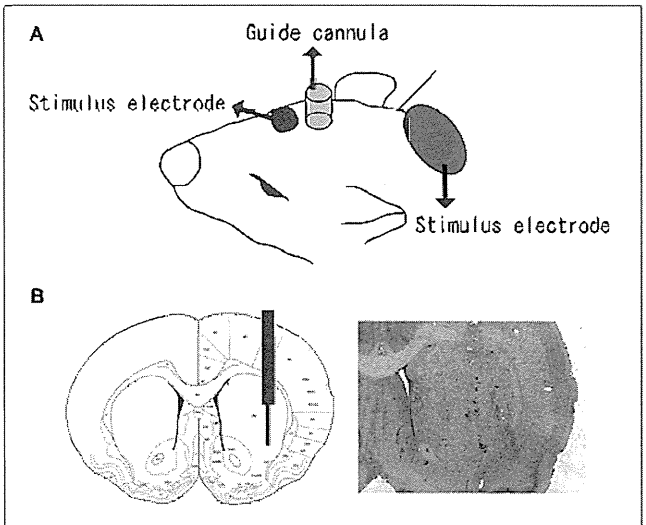

FIGURE 1 | Position of tDCS electrode and microdialysis probe. (A) One electrode (small red square) of the stimulator was fixed to the skin with surgical tape just above the brain region including the cortex. The anatomical location corresponded to +2.0 to +7.0 mm anterior and +1.0 to +6.0 mm lateral to the bregma. A second electrode (large red ellipse) was placed on the neck. A guide cannula (blue cylinder) was fixed to the skull with resin dental cement. **(B)** a microdialysis probe was inserted into the striatum (+1.0 mm anterior, +3.5 mm lateral, and −4.5 mm ventral to the bregma)

stimulation (Liebetanz et al., 2009), although the safety limits of anodal stimulation was not specified.

DOPAMINE AND SEROTONIN MEASUREMENTS

Stimulation and *in vivo* microdialysis were carried out under urethane anesthesia. Body temperature and heart rate were monitored and remained at approximately 37°C and 350 bpm, respectively. No remarkable changes in vigilance were observed by visual inspection of body movement. After surgery, microdialysis probes (AI-6-02; 2-mm membrane length; Eicom Corporation) were slowly inserted into the striatum through the guide cannula (**Figure 1B**). The probe was perfused continuously at a flow rate of 2 μl/min with artificial cerebrospinal fluid (aCSF) containing 0.9 mM $MgCl_2$, 147.0 mM NaCl, 4.0 mM KCl, and 1.2 mM $CaCl_2$. The collection and analysis of perfusion solution were performed at 10 min intervals over the duration of the experiment. The concentrations were judged stable when the fluctuation range of extracellular dopamine and serotonin levels did not exceed ±5% during six consecutive fractions and when there was not unidirectional fluctuation over more than three fractions (Alex et al., 2005; Kitaichi et al., 2010). After confirming the stability, three fractions were collected from the rat striatum before the application of tDCS as a baseline. Following tDCS, dialysis samples were collected every 10 min until at least 400 min after the onset of stimulation.

Dialysis fractions were analyzed using high-performance liquid chromatography (HPLC) with an electrochemical detection (ECD) system (Eicom Corporation). The extracellular serotonin level in the striatum was also measured, as it is known to be associated with the dopamine level (Di Giovanni et al., 2008; Navailles and De Deurwaerdere, 2011). Dopamine and serotonin were separated by a column with a mobile phase containing 99% 0.1 M sodium phosphate buffer (pH 6.0), 500 mg/L sodium 1-decanesulfonate, 50 mg/L ethylenediaminetetraacetic acid disodium salt (EDTA-2Na), and 1% methanol. The mobile phase was delivered at a flow rate of 500 μl/min. Before every experiment dopamine hydrochloride and serotonin hydrochloride, as the standard reagents, were dissolved in solvent and injected into the HPLC system. Retention times of dopamine and serotonin were calculated from the peaks detected in the chromatograph. During each experiment, the retention time of substances, which were collected from the striatum, was calculated. When the measured retention time matched with those of the standard reagents, collected substances were judged as dopamine or serotonin. All the measurement conditions such as mobile phase for calibration were same as those for actual measurements of rats. Dopamine and serotonin were quantified by calculating the peak areas (Alex et al., 2005; Kitaichi et al., 2010).

To confirm the insertion position of the microdialysis probe after completion of the experiment, all rats were deeply anesthetized with sodium pentobarbital (50 mg/kg body weight, i.p.) and perfused through the heart sequentially with 1 × phosphate buffered saline (PBS) followed by 10% formalin neutral buffer solution. Rat brains were post-fixed and sucrose-substituted at 4°C, and 20−μm-thick coronal sections were cut through the striatum (−1 mm to 3 mm anterior to the bregma) on a cryostat. These were then thaw-mounted on 3-aminopropyltriethoxysilane (APTS)-coated slides and stained with cresyl violet using standard procedures.

tDCS-INDUCED TISSUE DAMAGE

Histological examination was performed to determine the effects of tDCS on the brain tissue and skin beneath the scalp electrode. At 24 h after the application of tDCS, 12 rats (cathodal tDCS and sham groups; $n = 6$ per group) were deeply anesthetized with sodium pentobarbital (50 mg/kg body weight, i.p.), and 10−μm-thick coronal sections of their brains were prepared and stained with cresyl violet using a method similar to that described above. The skins were post-fixed at 4°C, dehydrated with ethanol and xylene, and paraffin-embedded. Sections (5−μm thick) of rat skin from just below the scalp electrode were cut on a microtome, thaw-mounted on APTS-coated slides, and stained with hematoxylin and eosin (HE) using standard procedures. Morphological changes were then evaluated. To confirm whether tDCS leads to apoptosis, 10−μm-thick coronal sections were prepared from the same animals and stained with terminal deoxynucleotidyl transferase-mediated biotinylated UTP nick-end labeling (TUNEL) (Kobayashi et al., 2004). To minimize the number of animals used in the experiments, we omitted the anodal tDCS group, which showed no significant changes in dopamine or serotonin levels in the microdialysis experiment (see section Results).

STATISTICAL ANALYSIS

Data from four rats in which a probe had not been accurately inserted into the striatum (**Figure 1B**) were excluded from statistical analysis. Extracellular dopamine and serotonin levels were expressed as percentage signal changes from baseline values before tDCS application. Group data are presented as mean ± standard error (*SEM*). The statistical significance of differences between groups was assessed by repeated measures analysis of variance (ANOVA) with time (TIME) as a within-subject factor and group (GROUP) as a between-subject factor. This was followed by the *post-hoc* Bonferroni test using SPSS software (SPSS Inc., Chicago, IL). To investigate whether the time effect differed between groups, we confirmed the "TIME" × "GROUP" interaction. *P*-values less than 5% were considered statistically significant. To investigate when the change in dopamine level became prominent, data at each time point were compared with the baseline using the paired *t*-tests. For the same purpose, data from the tDCS group were compared with those in the sham group at each time point separately using the unpaired two-sample *t*-tests.

RESULTS

Statistical analysis was carried out on rats in the cathodal tDCS ($n = 7$), anodal tDCS ($n = 7$), and sham ($n = 7$) groups. To examine whether cathodal or anodal tDCS affected extracellular dopamine and serotonin levels in the striatum, we investigated the effect of tDCS using *in vivo* microdialysis. The absolute basal dialysis levels of dopamine and serotonin detected 10 min before the interventions did not differ between the three groups [**Table 1**; dopamine, $F_{(2, 20)} = 0.389$, $p = 0.684$; serotonin, $F_{(2, 20)} = 0.242$, $p = 0.788$]. These basal levels compared well with the previous studies (Baumann et al., 2008; Kitaichi

et al., 2010). Following the application of cathodal tDCS for 10 min, the extracellular dopamine levels continuously increased and this effect lasted for more than 400 min after the stimulation ceased (**Figure 2**).

The dopamine time-course in the striatum differed significantly between the three groups [main effect of GROUP, $F_{(1,\ 20)} = 27.386$, $p < 0.001$; main effect of TIME, $F_{(44,\ 880)} = 0.514$, $p = 0.997$; interaction of GROUP × TIME, $F_{(2,\ 88)} = 4.674$, $p < 0.001$]. The dopamine increases in the cathodal tDCS group were significantly greater than those in the sham and the anodal tDCS groups ($p < 0.001$ for both, *post-hoc* test). These increases became statistically prominent 120 min after the stimulation compared with the pre-intervention period ($p < 0.05$, paired *t*-test), and lasted throughout the observation period. Furthermore, the dopamine increases in the cathodal tDCS group were significantly greater than those in the sham group from 120 min after stimulation ($p < 0.05$, unpaired two-sample *t*-test). By contrast, the application of anodal tDCS did not induce significant increases in extracellular dopamine levels.

Table 1 | Absolute basal dialysis levels of dopamine and serotonin.

Group	Dopamine (nM)	Serotonin (nM)
Sham	0.61 ± 0.070	0.11 ± 0.076
Cathodal tDCS	0.62 ± 0.076	0.11 ± 0.062
Anodal tDCS	0.69 ± 0.071	0.06 ± 0.012

Data are presented as the mean ± SEM.

There were no significant changes in extracellular serotonin levels in the striatum in any group, indicating that they were unaffected by the application of either cathodal or anodal tDCS [**Figure 3**; main effect of GROUP, $F_{(1,\ 20)} = 2.016$, $p = 0.159$; interaction of GROUP × TIME, $F_{(2,\ 86)} = 0.997$, $p = 0.540$, respectively].

One day after the application of tDCS, tissues were dissected and processed for sectioning. The sections through the cortex were used for histological examination with cresyl violet staining. No abnormal findings regarding cellular morphology, such as chromatolysis or atrophied tissue, were observed in the cortex below the scalp electrode of rats in either the cathodal tDCS group or the sham group (**Figure 4A**). No apoptosis was found in either group (data not shown). The sections through the skin below the scalp electrode were analyzed by HE staining, revealing no abnormalities such as dead tissue, inclusion, or multicell spheroids in either group (**Figure 4B**).

DISCUSSION

The main finding of the present study was that cathodal tDCS induced a significant increase in extracellular dopamine levels in the rat striatum, whereas anodal tDCS in the same area had no effect. Although recent magnetic-resonance spectroscopy studies have shown direct effects of tDCS on cortical GABA concentration (Stagg et al., 2009), the effect of tDCS on subcortical neurotransmitters has remained unclear. The present results suggest that tDCS has a direct and/or indirect effect on the dopaminergic system in the basal ganglia. The finding that tDCS affected dopamine but not serotonin is consistent with a

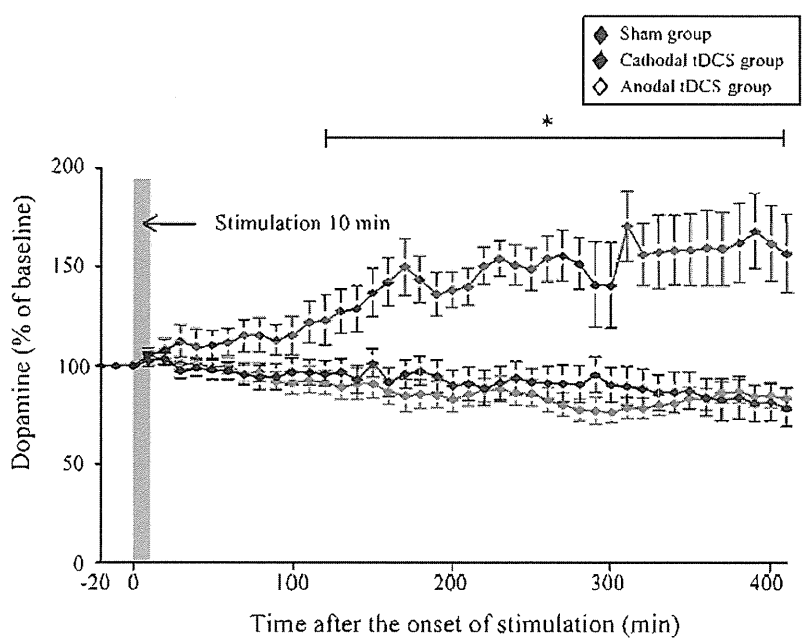

FIGURE 2 | Effect of tDCS on extracellular dopamine levels in the striatum. The absolute basal dialysis levels of dopamine in the striatum detected 10 min before the interventions did not differ between groups. Dopamine levels were expressed as percentage signal changes from baseline values before the tDCS application. Group data are presented as the mean ± *SEM*. Cathodal, but not anodal, tDCS significantly increased extracellular dopamine levels in the striatum. *$p < 0.001$

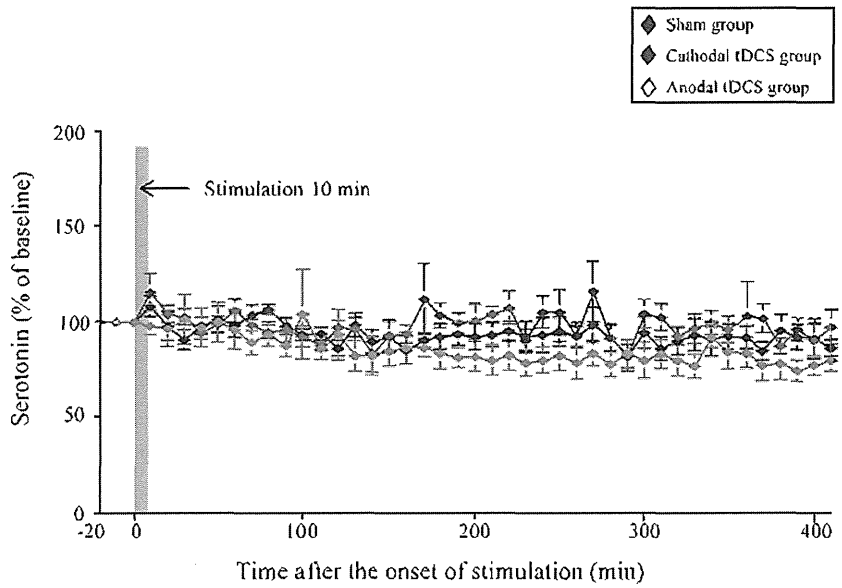

FIGURE 3 | Effect of tDCS on extracellular serotonin levels in the striatum. The absolute basal dialysis levels of serotonin in the striatum detected 10 min before the interventions did not differ between groups. Serotonin levels were expressed as percentage signal changes from baseline values before the tDCS application. Group data are presented as the mean ± *SEM*. None of the tDCS applications significantly affected extracellular serotonin levels

previous study that reported no changes in the rat serotonergic system following repetitive transcranial magnetic stimulation (rTMS) (Kanno et al., 2004). As the tDCS methods used here did not damage tissue in the cortex or the skin below the scalp electrode, it is unlikely that the rise in dopamine was induced by non-specific cellular injury.

INTERPRETATION OF THE CATHODAL tDCS EFFECT

Several studies have shown that diverse areas of the cerebral cortex, including the sensory, motor, and associated regions, project to the subcortical regions, including the striatum (McGeorge and Faull, 1989; Lang et al., 2005; Halko et al., 2011). Furthermore, it has been reported that descending pathways from the frontal cortex to the striatum modulate a release of dopamine in subcortical areas in both animal and human experiments (Murase et al., 1993; Taber and Fibiger, 1995; Karreman and Moghaddam, 1996). Considering that tDCS has been found to improve symptoms of PD in both animal and human experiments (Boggio et al., 2006; Fregni et al., 2006; Benninger et al., 2010; Gruner et al., 2010; Li et al., 2011), it is plausible that tDCS could directly and/or indirectly affect the extracellular dopamine levels in the striatum.

However, our finding that cathodal tDCS, but not anodal, increased extracellular dopamine levels is contradictory to our prediction and inconsistent with previous studies. For example, cathodal tDCS has been thought to induce suppression of motor function and learning by inhibiting neuronal excitability of the cortex (Murphy et al., 2009; Nitsche et al., 2009; Bachmann et al., 2010; Benninger et al., 2010; Fox, 2011; Schambra et al., 2011; Tanaka et al., 2011a). In addition, rTMS has been suggested to induce increased extracellular dopamine levels in the striatum by facilitating neuronal excitability of the cortex (Keck et al., 2002; Strafella et al., 2003; Ohnishi et al., 2004). We acknowledge that the present finding is contradictory to such studies.

To our knowledge, this is the first report that directly measured extracellular dopamine levels in the striatum-induced by tDCS. Although the mechanism underlying the long-lasting effect of cathodal tDCS observed in the present study has not yet been determined, we offer the following speculations. It has been widely accepted that cathodal tDCS decreases cortical neuronal activity (Bindman et al., 1964; Purpura and McMurtry, 1965; Fritsch et al., 2010). Meanwhile, a recent report showed that cathodal, but not anodal, tDCS induced paired pulse facilitation in the somatosensory cortex of rabbits following stimulation of the ventroposterior medial thalamic nucleus (Marquez-Ruiz et al., 2012). This study suggests that cathodal tDCS may specifically facilitate synaptic plasticity. Furthermore, cathodal, but not anodal, tDCS was shown to facilitate working memory and skill learning 21 days after treatment, implying that cathodal tDCS might facilitate long-term homeostatic cortical metaplasticity (Dockery et al., 2011). Although the cathodal tDCS may instantaneously decrease neuronal activity beneath the stimulus electrode, these findings suggest that cathodal tDCS may specifically induce a long-term plastic change thorough some metabolic changes, such as BDNF release (Fritsch et al., 2010). We speculate that the increase of dopamine release in the striatum may contribute to such long-term plasticity.

Alternatively, the cortico-basal ganglia neural circuit contains both excitatory and inhibitory projections (Alexander and Crutcher, 1990; Nambu et al., 2000) in an intrinsic neuronal network. Therefore, we must also consider the possibility that cathodal tDCS affects extracellular dopamine levels in the striatum through an inhibitory circuit.

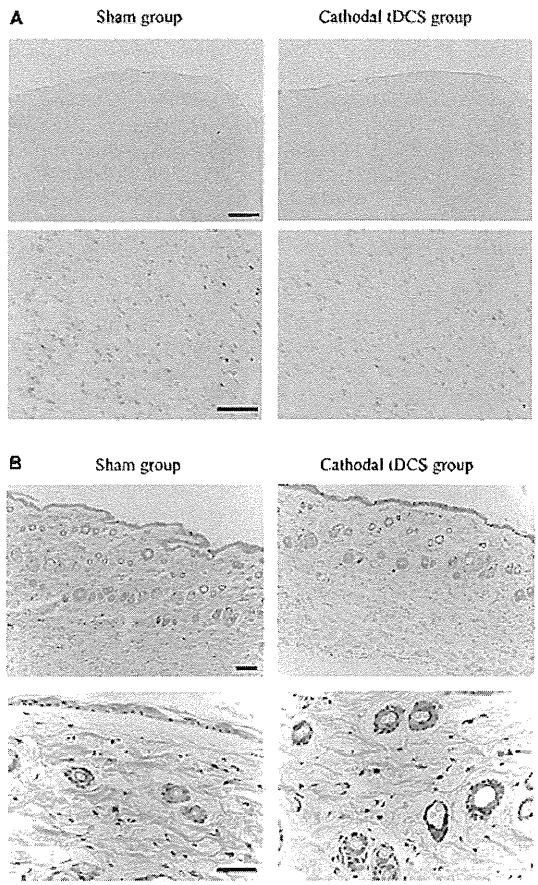

FIGURE 4 | Histological examination following tDCS. (A) Cresyl violet staining of the brain tissue below the scalp electrode in the sham group (left) and the cathodal tDCS group (right) 24 h after tDCS application. Scale bars 1 mm for upper panels, 100 μm for lower panels; **(B)** HE staining of the skin below the scalp electrode in the sham group (left) and the cathodal tDCS group (right) 24 h after tDCS application. Scale bars: 100 μm for upper panels, 50 μm for lower panels. No morphological change was observed in brain tissue and skin.

EXPERIMENTAL LIMITATIONS

General anesthesia affects brain metabolism, neuronal activity, and response to sensory stimuli (Buzsaki et al., 1983; Friedberg et al., 1999); it is thus conceivable that the present results were partly influenced by anesthesia. However, this is unlikely to be the only reason for the cathodal tDCS-specific dopamine increase, as the anesthetic procedure was common to all stimulation conditions. Moreover, in a previous study, alteration of extracellular dopamine levels in the striatum induced by medial forebrain bundle stimulation did not differ between urethane-anesthetized and awake animals (Tepper et al., 1991).

The contamination effect induced by the tDCS reference electrode on the neck should be considered. Although the electrode-current density in this region was lower and less effective, and there is no brain tissue beneath the tDCS reference electrode on the neck, it was unclear exactly how the current flowed between the two electrodes in the present experimental setup. Furthermore, the current delivered by the stimulation electrode might have reached the striatum through the guide cannula, even though the dental cement used to fix it was an electrical insulator. To rule out this possibility, extracellular dopamine levels should be measured using a non-invasive technique such as positron-emission tomography.

Though polarity of their affective stimulation electrode differed from that of the present study, some reports have shown that tDCS improves PD symptoms in both animals and humans (Boggio et al., 2006; Fregni et al., 2006; Benninger et al., 2010; Gruner et al., 2010; Li et al., 2011). An underlying mechanism of such clinical effects could be an increase in extracellular dopamine levels in the striatum induced by tDCS. However, it is as of yet unclear whether 150% of basal dopamine level is clinically relevant and if tDCS will increase dopamine levels in patients whose dopaminergic neurons have degenerated. Therefore, we recommend caution in correlating the present finding to clinical application of tDCS.

In conclusion, we demonstrated that cathodal tDCS increased extracellular dopamine levels in the rat striatum. This suggests that tDCS has a direct and/or indirect effect on the dopaminergic system in the subcortical area. Further work to determine the mechanism underlying tDCS effects on cortical-basal ganglia functions could benefit our understanding of learning-induced neuroplasticity and the development of new clinical interventions.

AUTHOR CONTRIBUTIONS

Tomoko Tanaka, Yuji Takano, Satoshi Tanaka, Naoyuki Hironaka, Kazuto Kobayashi, Takashi Hanakawa, Katsumi Watanabe, and Manabu Honda designed the research; Tomoko Tanaka performed the research; Tomoko Tanaka analyzed the data; Tomoko Tanaka, Satoshi Tanaka, and Manabu Honda wrote the paper.

ACKNOWLEDGMENTS

We thank S. Shimojo and T. Nishikawa for comments on this work. This work was partly supported by JSPS KAKENHI Grant Number 22240049 and by MEXT KAKENHI Grant Number 22135008 for Manabu Honda and by JST for Naoyuki Hironaka and Katsumi Watanabe.

REFERENCES

Adcock, R. A., Thangavel, A., Whitfield-Gabrieli, S., Knutson, B., and Gabrieli, J. D. (2006). Reward-motivated learning: mesolimbic activation precedes memory formation. *Neuron* 50, 507–517.

Alex, K. D., Yavanian, G. J., McFarlane, H. G., Pluto, C. P., and Pehek, E A. (2005). Modulation of dopamine release by striatal 5-HT2C receptors. *Synapse* 55, 242–251.

Alexander, G. E., and Crutcher, M. D. (1990). Functional architecture of basal ganglia circuits: neural substrates of parallel processing. *Trends Neurosci.* 13, 266–271.

Antal, A., Polania, R., Schmidt-Samoa, C., Dechent, P., and Paulus, W. (2011). Transcranial direct current stimulation over the primary motor cortex during fMRI. *Neuroimage* 55, 590–596.

Bachmann, C. G., Muschinsky, S., Nitsche, M. A., Rolke, R., Magerl, W., Treede, R. D., et al. (2010). Transcranial direct current stimulation of the motor cortex induces distinct changes in thermal and mechanical sensory percepts. *Clin. Neurophysiol.* 121, 2083–2089.

Baumann, M. H., Clark, R. D., and Rothman, R. B. (2008). Locomotor stimulation produced by 3, 4-methylenedioxymethamphetamine (MDMA) is correlated with dialysate levels of serotonin and dopamine in rat brain. *Pharmacol. Biochem. Behav.* 90, 208–217.

Benninger, D. H., Lomarev, M., Lopez, G., Wassermann, E. M., Li, X., Considine, E., et al. (2010). Transcranial direct current stimulation for the treatment of Parkinson's disease. *J. Neurol. Neurosurg. Psychiatry* 81, 1105–1111.

Berridge, K. C. (2007). The debate over dopamine's role in reward: the case for incentive salience. *Psychopharmacology (Berl.)* 191, 391–431.

Bindman, L. J., Lippold, O. C., and Redfearn, J. W. (1964). The action of brief polarizing currents on the cerebral cortex of the rat (1) during current flow and (2) in the production of long-lasting after-effects. *J. Physiol.* 172, 369–382.

Binkofski, F., Lochig, M., Jauch-Chara, K., Bergmann, S., Melchert, U. H., Scholand-Engler, H. G., et al. (2011). Brain energy consumption induced by electrical stimulation promotes systemic glucose uptake. *Biol. Psychiatry* 70, 690–695.

Boggio, P. S., Ferrucci, R., Rigonatti, S. P., Covre, P., Nitsche, M., Pascual-Leone, A., et al. (2006). Effects of transcranial direct current stimulation on working memory in patients with Parkinson's disease. *J. Neurol. Sci.* 249, 31–38.

Brunoni, A. R., Nitsche, M. A., Bolognini, N., Bikson, M., Wagner, T., Merabet, L., et al. (2012). Clinical research with transcranial direct current stimulation (tDCS): challenges and future directions. *Brain Stimul.* 5, 175–195.

Buzsaki, G., Leung, L. W., and Vanderwolf, C. H. (1983). Cellular bases of hippocampal EEG in the behaving rat. *Brain Res.* 287, 139–171.

Carlsson, A. (1972). Biochemical and pharmacological aspects of Parkinsonism. *Acta Neurol. Scand. Suppl.* 51, 11–42.

Di Giovanni, G., Di Matteo, V., Pierucci, M., and Esposito, E. (2008). Serotonin-dopamine interaction: electrophysiological evidence. *Prog. Brain Res.* 172, 45–71.

Dockery, C. A., Liebetanz, D., Birbaumer, N., Malinowska, M., and Wesierska, M. J. (2011). Cumulative benefits of frontal transcranial direct current stimulation on visuospatial working memory training and skill learning in rats. *Neurobiol. Learn. Mem.* 96, 452–460.

Ebrahimi, A., Pocher, R., and Roger, M. (1992). Topographical organization of the projections from physiologically identified areas of the motor cortex to the striatum in the rat. *Neurosci. Res.* 14, 39–60.

Fahn, S. (2003). Description of Parkinson's disease as a clinical syndrome. *Ann. N.Y. Acad. Sci.* 991, 1–14.

Fox, D. (2011). Neuroscience: brain buzz. *Nature* 472, 156–158.

Fregni, F., Boggio, P. S., Santos, M. C., Lima, M., Vieira, A. L., Rigonatti, S. P., et al. (2006). Noninvasive cortical stimulation with transcranial direct current stimulation in Parkinson's disease. *Mov. Disord.* 21, 1693–1702.

Friedberg, M. H., Lee, S. M., and Ebner, F. F. (1999). Modulation of receptive field properties of thalamic somatosensory neurons by the depth of anesthesia. *J. Neurophysiol.* 81, 2243–2252.

Fritsch, B., Reis, J., Martinowich, K., Schambra, H. M., Ji, Y., Cohen, L. G., et al. (2010). Direct current stimulation promotes BDNF-dependent synaptic plasticity: potential implications for motor learning. *Neuron* 66, 198–204.

Gabbott, P. L., Warner, T. A., Jays, P. R., Salway, P., and Busby, S. J. (2005). Prefrontal cortex in the rat: projections to subcortical autonomic, motor, and limbic centers. *J. Comp. Neurol.* 492, 145–177.

Gruner, U., Eggers, C., Ameli, M., Sarfeld, A. S., Fink, G. R., and Nowak, D. A. (2010). 1 Hz rTMS preconditioned by tDCS over the primary motor cortex in Parkinson's disease: effects on bradykinesia of arm and hand. *J. Neural Transm.* 117, 207–216.

Halko, M. A., Datta, A., Plow, E. B., Scaturro, J., Bikson, M., and Merabet, L. B. (2011). Neuroplastic changes following rehabilitative training correlate with regional electrical field induced with tDCS. *Neuroimage* 57, 885–891.

Hummel, F., Celnik, P., Giraux, P., Floel, A., Wu, W. H., Gerloff, C., et al. (2005). Effects of non-invasive cortical stimulation on skilled motor function in chronic stroke. *Brain* 128, 490–499.

Kanno, M., Matsumoto, M., Togashi, H., Yoshioka, M., and Mano, Y. (2004). Effects of acute repetitive transcranial magnetic stimulation on dopamine release in the rat dorsolateral striatum. *J. Neurol. Sci.* 217, 73–81.

Karreman, M., and Moghaddam, B. (1996). The prefrontal cortex regulates the basal release of dopamine in the limbic striatum: an effect mediated by ventral tegmental area. *J. Neurochem.* 66, 589–598.

Keck, M. E., Welt, T., Muller, M. B., Erhardt, A., Ohl, F., Toschi, N., et al. (2002). Repetitive transcranial magnetic stimulation increases the release of dopamine in the mesolimbic and mesostriatal system. *Neuropharmacology* 43, 101–109.

Keeser, D., Meindl, T., Bor, I., Palm, U., Pogarell, O., Mulert, C., et al. (2011). Prefrontal transcranial direct current stimulation changes connectivity of resting-state networks during fMRI. *J. Neurosci.* 31, 15284–15293.

Kim, S. J., Kim, B. K., Ko, Y. J., Bang, M. S., Kim, M. H., and Han, T. R. (2010). Functional and histologic changes after repeated transcranial direct current stimulation in rat stroke model. *J. Korean Med. Sci.* 25, 1499–1505.

Kitaichi, Y., Inoue, T., Nakagawa, S., Boku, S., Kakuta, A., Izumi, T., et al. (2010). Sertraline increases extracellular levels not only of serotonin, but also of dopamine in the nucleus accumbens and striatum of rats. *Eur. J. Pharmacol.* 647, 90–96.

Kobayashi, K., Takahashi, M., Matsushita, N., Miyazaki, J., Koike, M., Yaginuma, H., et al. (2004). Survival of developing motor neurons mediated by Rho GTPase signaling pathway through Rho-kinase. *J. Neurosci.* 24, 3480–3488.

Lang, N., Siebner, H. R., Ward, N. S., Lee, L., Nitsche, M. A., Paulus, W., et al. (2005). How does transcranial DC stimulation of the primary motor cortex alter regional neuronal activity in the human brain? *Eur. J. Neurosci.* 22, 495–504.

Laste, G., Caumo, W., Adachi, L. N., Rozisky, J. R., De Macedo, I. C., Filho, P. R., et al. (2012). After-effects of consecutive sessions of transcranial direct current stimulation (tDCS) in a rat model of chronic inflammation. *Exp. Brain Res.* 221, 75–83.

Lefaucheur, J. P. (2009). Methods of therapeutic cortical stimulation. *Neurophysiol. Clin.* 39, 1–14.

Li, Y., Tian, X., Qian, L., Yu, X., and Jiang, W. (2011). Anodal transcranial direct current stimulation relieves the unilateral bias of a rat model of Parkinson's disease. *Conf. Proc. IEEE Eng. Med. Biol. Soc.* 2011, 765–768.

Liebetanz, D., Koch, R., Mayenfels, S., Konig, F., Paulus, W., and Nitsche, M. A. (2009). Safety limits of cathodal transcranial direct current stimulation in rats. *Clin. Neurophysiol.* 120, 1161–1167.

Liebetanz, D., Nitsche, M. A., Tergau, F., and Paulus, W. (2002). Pharmacological approach to the mechanisms of transcranial DC-stimulation-induced after-effects of human motor cortex excitability. *Brain* 125, 2238–2247.

Marquez-Ruiz, J., Leal-Campanario, R., Sanchez-Campusano, R., Molaee-Ardekani, B., Wendling, F., Miranda, P. C., et al. (2012). Transcranial direct-current stimulation modulates synaptic mechanisms involved in associative learning in behaving rabbits. *Proc. Natl. Acad. Sci. U.S.A.* 109, 6710–6715.

McGeorge, A. J., and Faull, R. L. (1989). The organization of the projection from the cerebral cortex to the striatum in the rat. *Neuroscience* 29, 503–537.

Murase, S., Grenhoff, J., Chouvet, G., Gonon, F. G., and Svensson, T. H. (1993). Prefrontal cortex regulates burst firing and transmitter release in rat mesolimbic dopamine neurons studied *in vivo*. *Neurosci. Lett.* 157, 53–56.

Murphy, D. N., Boggio, P., and Fregni, F. (2009). Transcranial direct current stimulation as a therapeutic tool for the treatment of major depression: insights from past and recent clinical studies. *Curr. Opin. Psychiatry* 22, 306–311.

Nambu, A., Tokuno, H., Hamada, I., Kita, H., Imanishi, M., Akazawa, T., et al. (2000). Excitatory cortical inputs to pallidal neurons via the subthalamic nucleus in the monkey. *J. Neurophysiol.* 84, 289–300.

Navailles, S., and De Deurwaerdere, P. (2011). Presynaptic control of serotonin on striatal dopamine function. *Psychopharmacology (Berl.)* 213, 213–242.

Navailles, S., De Deurwaerdere, P., Porras, G., and Spampinato, U. (2004). *In vivo* evidence that 5-HT2C receptor antagonist but not agonist modulates cocaine-induced dopamine outflow in the rat nucleus accumbens and striatum. *Neuropsychopharmacology* 29, 319–326.

Nitsche, M. A., Boggio, P. S., Fregni, F., and Pascual-Leone, A. (2009). Treatment of depression with transcranial direct current stimulation (tDCS): a review. *Exp. Neurol.* 219, 14–19.

Nitsche, M. A., Fricke, K., Henschke, U., Schlitterlau, A., Liebetanz, D., Lang, N., et al. (2003). Pharmacological modulation of cortical excitability shifts induced by transcranial direct current stimulation in humans. *J. Physiol.* 553, 293–301.

Nitsche, M. A., Lampe, C., Antal, A., Liebetanz, D., Lang, N., Tergau, F.,

et al. (2006). Dopaminergic modulation of long-lasting direct current-induced cortical excitability changes in the human motor cortex. *Eur. J. Neurosci.* 23, 1651–1657.

Nitsche, M. A., and Paulus, W. (2000). Excitability changes induced in the human motor cortex by weak transcranial direct current stimulation. *J. Physiol.* 527(Pt 3), 633–639.

Ohnishi, T., Hayashi, T., Okabe, S., Nonaka, I., Matsuda, H., Iida, H., et al. (2004). Endogenous dopamine release induced by repetitive transcranial magnetic stimulation over the primary motor cortex: an [11C]raclopride positron emission tomography study in anesthetized macaque monkeys. *Biol. Psychiatry* 55, 484–489.

Paxinos, G., and Watson, C. (1998). *The Rat Brain in Stereotaxic Coordinates.* San Diego, CA: Academic Press.

Purpura, D. P., and McMurtry, J. G. (1965). Intracellular activities and evoked potential changes during polarization of motor cortex. *J. Neurophysiol.* 28, 166–185.

Rossato, J. I., Bevilaqua, L. R., Izquierdo, I., Medina, J. H., and Cammarota, M. (2009). Dopamine controls persistence of long-term memory storage. *Science* 325, 1017–1020.

Schambra, H. M., Abe, M., Luckenbaugh, D. A., Reis, J., Krakauer, J. W., and Cohen, L. G. (2011). Probing for hemispheric specialization for motor skill learning: a transcranial direct current stimulation study. *J. Neurophysiol.* 106, 652–661.

Selemon, L. D., and Goldman-Rakic, P. S. (1985). Longitudinal topography and interdigitation of corticostriatal projections in the rhesus monkey. *J. Neurosci.* 5, 776–794.

Stagg, C. J., Best, J. G., Stephenson, M. C., O'Shea, J., Wylezinska, M., Kincses, Z. T., et al. (2009). Polarity-sensitive modulation of cortical neurotransmitters by transcranial stimulation. *J. Neurosci.* 29, 5202–5206.

Strafella, A. P., Paus, T., Fraraccio, M., and Dagher, A. (2003). Striatal dopamine release induced by repetitive transcranial magnetic stimulation of the human motor cortex. *Brain* 126, 2609–2615.

Taber, M. T., and Fibiger, H. C. (1995). Electrical stimulation of the prefrontal cortex increases dopamine release in the nucleus accumbens of the rat: modulation by metabotropic glutamate receptors. *J. Neurosci.* 15, 3896–3904.

Takano, Y., Yokawa, T., Masuda, A., Niimi, J., Tanaka, S., and Hironaka, N. (2010). A rat model for measuring the effectiveness of transcranial direct current stimulation using fMRI. *Neurosci. Lett.* 491, 40–43.

Tanaka, S., Hanakawa, T., Honda, M., and Watanabe, K. (2009). Enhancement of pinch force in the lower leg by anodal transcranial direct current stimulation. *Exp. Brain Res.* 196, 459–465.

Tanaka, S., Sandrini, M., and Cohen, L. G. (2011a). Modulation of motor learning and memory formation by non-invasive cortical stimulation of the primary motor cortex. *Neuropsychol. Rehabil.* 21, 650–675.

Tanaka, T., Kai, N., Kobayashi, K., Takano, Y., and Hironaka, N. (2011b). Up-regulation of dopamine D1 receptor in the hippocampus after establishment of conditioned place preference by cocaine. *Neuropharmacology* 61, 842–848.

Tepper, J. M., Creese, I., and Schwartz, D. H. (1991). Stimulus-evoked changes in neostriatal dopamine levels in awake and anesthetized rats as measured by microdialysis. *Brain Res.* 559, 283–292.

Veening, J. G., Cornelissen, F. M., and Lieven, P. A. (1980). The topical organization of the afferents to the caudatoputamen of the rat. A horseradish peroxidase study. *Neuroscience* 5, 1253–1268.

Wachter, D., Wrede, A., Schulz-Schaeffer, W., Taghizadeh-Waghefi, A., Nitsche, M. A., Kutschenko, A., et al. (2011). Transcranial direct current stimulation induces polarity-specific changes of cortical blood perfusion in the rat. *Exp. Neurol.* 227, 322–327.

Wassermann, E. M., and Grafman, J. (2005). Recharging cognition with DC brain polarization. *Trends Cogn. Sci.* 9, 503–505.

Conflict of Interest Statement: The authors declare that the research was conducted in the absence of any commercial or financial relationships that could be construed as a potential conflict of interest.

Received: 04 December 2012; accepted: 16 March 2013, published online: 11 April 2013.

Citation: Tanaka T, Takano Y, Tanaka S, Hironaka N, Kobayashi K, Hanakawa T, Watanabe K and Honda M (2013) Transcranial direct-current stimulation increases extracellular dopamine levels in the rat striatum. Front. Syst. Neurosci. 7:6. doi: 10.3389/fnsys.2013.00006

Oohashi, Tsutomu, Tadao Maekawa, Osamu Ueno, Norie Kawai, Emi Nishina, & Manabu Honda. 2013. Evolutionary acquisition of a mortal genetic program: The origin of an altruistic gene. *Artificial Life*, uncorrected proof.

Evolutionary Acquisition of a Mortal Genetic Program: The Origin of an Altruistic Gene

Tsutomu Oohashi[*,**,†]
Foundation for Advancement of International Science

Tadao Maekawa[*,**,‡]
Yokkaichi University

Osamu Ueno[§]
National Center of Neurology and Psychiatry
CREST, Japan Science and Technology Agency

Norie Kawai[†]
Foundation for Advancement of International Science
Waseda University

Emi Nishina[¶]
Center of ICT
Distance Education, The Open University of Japan
The Graduate University for Advanced Studies

Manabu Honda[§]
National Center of Neurology and Psychiatry
CREST, Japan Science and Technology Agency

Abstract As part of our research on programmed self-decomposition, we formed the hypothesis that originally immortal terrestrial organisms evolve into ones that are programmed for autonomous death. We then conducted evolutionary simulation experiments in which we examined this hypothesis using an artificial ecosystem that we designed to resemble a terrestrial ecosystem endowed with artificial chemistry. Notable results corroborating our hypothesis were obtained, which showed that mortal organisms emerged from indigenous immortal organisms through mutation; such mortal organisms survived and left behind offspring, albeit very rarely, and, having survived, surpassed immortal organisms without exception. In this article, we report the details of the above findings and also discuss a background framework we previously constructed for approaching altruism.

Keywords
Altruism, cooperation, programmed self-decomposition (PSD), programmed death, autolysis, terrestrial life, artificial chemistry (AChem)

A version of this paper with color figures is available online at http://dx.doi.org/10.1162/artl_a_00098. Subscription required.

* Contact author.
** These authors have contributed equally to this article.
† Department of Research and Development, Foundation for Advancement of International Science, 3-24-16 Kasuga, Tsukuba, Ibaraki 305-0821, Japan. E-mail: oohashi@fais.or.jp (T.O.); nkawai@fais.or.jp (N.K.)
‡ Faculty of Environmental and Information Sciences, Yokkaichi University, 1200 Kayou-cho, Yokkaichi, Mie 512-8512, Japan. E-mail: maekawa@yokkaichi-u.ac.jp
§ Department of Functional Brain Research, National Center of Neurology and Psychiatry and CREST, Japan Science and Technology Agency, 4-1-1 Ogawahigashi, Kodaira, Tokyo 187-8502, Japan. E-mail: ueno-o@ncnp.go.jp (O.U.); honda@ncnp.go.jp (M.H.)
¶ Center of ICT and Distance Education, The Open University of Japan and School of Cultural and Social Studies, The Graduate University for Advanced Studies, 2-11 Wakaba, Mihama-ku, Chiba 261-8586 Japan. E-mail: nishina@ouj.ac.jp

1 Introduction

We previously modeled autonomous death, which is one of the significant and universal attributes of terrestrial life, as programmed self-decomposition (PSD) [18, 24]. Our research has proceeded by means of a series of studies that look into the existence of autonomous death through experiments in the field of molecular cell biology with existing living organisms as subjects; concurrently, through evolutionary simulations of artificial life (ALife), we raise the possibility that mortal organisms having autonomous death are superior to immortal organisms [9–11, 18–24, 26]. In doing so, we have meshed the following three approaches.

(1) *Model constitution:* As typically shown in many studies in the field of evolution, including those by Charles R. Darwin and William D. Hamilton, the research model often predetermines both the possibility and limitation of the study in question. We have therefore attempted to construct a new model for autonomous death based on cutting-edge techniques and a perspective that draws on various fields, including ALife and molecular cell biology, so as to extend to areas beyond the scope of previous models.

(2) *Verification of a model through comparison with real-life phenomena:* In carrying out a series of simple, straightforward experiments, we have deployed a concrete and sound approach drawing on the principles and methodology of molecular cell biology.

(3) *Simulation of evolution using artificial life as a critical tool:* In order to verify our evolutionary model, we had to deal with an extremely complex ecosystem on a large spatiotemporal scale that far exceeds observations of and experiments on real-life individuals. It would be impracticable to perform an evolutionary experiment in the real world, because that would require an earth-scale space and a million-year time span. In view of our research objectives, artificial life has provided the optimum alternative to real life for scientific inquiry. To obtain conclusive research results, we have integrated various interdisciplinary approaches through evolutionary simulations making use of artificial life. Below we introduce certain key points in our studies to provide background for the current study.

1.1 Programmed Self-Decomposition Model

The essence of our PSD model derives from the fact that we have zeroed in on autolysis, which is universally observed in terrestrial lives, including unicellular organisms, as phenomena involving autonomous material recycling in a terrestrial ecosystem.

Since a terrestrial ecosystem has a finite material environment, terrestrial lives require material recycling to maintain their life activities. Eugene P. Odum listed four principal pathways responsible for material recycling in his *Fundamentals of Ecology* [17] as follows: (i) primary animal excretion; (ii) microbial decomposition of detritus; (iii) direct cycling from plant to plant through symbiotic microorganisms; and (iv) autolysis. Autolysis as treated by Odum has been conventionally regarded as uncontrollable, natural disintegration with increasing entropy. We have redefined autolysis as a kind of autonomous, altruistic phenomenon beneficial to an ecosystem, in part and as a whole [18]. We thus regard autolysis as an active biochemical process built into cellular genetic programming by which a cell consumes its own metabolic energy. In accordance with this autolytic process, we posit that living individuals autonomously decompose themselves into components; in particular, cells hydrolyze biological polymers into biological monomers so that the materials that they used and the spaces where they existed can be optimally reutilized by all other living individuals, including adversaries and competitors, and by that means can return to the environment and thus contribute to the restoration of the entire ecosystem. Regarding the concept of altruism that we have utilized as a tool for these studies, we have partially revised the conventional concept, as discussed in Section 4.

We venture to posit that this phenomenon is built into each single cell, which is the fundamental unit of all terrestrial life, and that it takes place as the cell lives out its natural life span or whenever it

encounters an inadaptable environment. Therefore this phenomenon is inseparable from programmed cell death. In unicellular organisms this phenomenon is nothing other than individual autonomous death. At the level of individuals, it corresponds to complete abandonment of self-preservation and self-reproduction, and is indicative of complete withdrawal from and total renunciation of a struggle for existence, or of competition as a survival strategy. We refer to such a phenomenon as programmed self-decomposition (PSD) [18, 24].

In the field of molecular biology, it has recently been reported that autolysis involves certain active processes, including synthesis of new proteins, and is now regarded as a programmed active process [8, 29]. Additionally, necrosis of multicellular organisms, which corresponds to autolysis of unicellular organisms, might involve the regulated genetic program for cell death [2, 12]. Those recent studies support the concept of PSD from the viewpoint of molecular cell biology, which we previously proposed.

To express this concept in the form of an abstract, logical model completely removed from any and all concrete aspects of actual life activities, we constructed a mathematical model of life activities exemplified by self-reproduction and self-decomposition, taking John von Neumann's self-reproductive automaton [37] as our prototype and naming it the PSD model [18]. Details of this model are described elsewhere [18, 24].

1.2 Molecular Cell Biology Studies

It is of critical importance that our PSD model be applicable to actual terrestrial lives. We therefore adopted a eukaryotic unicellular organism, the protozoan *Tetrahymena*, as our experimental material, since it is highly conducive to mathematical modeling [18, 24]. For our impulse shock experimental model [24, 36]: First of all, we activated, for a short period of time, a genetic program with an external signal indicative of a fatal environment. Next, the culture condition was immediately restored to one appropriate for life, so that the physiological processes responsible for self-decomposition could proceed smoothly. To actualize our impulse shock model in a flask, we created concrete experimental conditions to induce the self-decomposition process. The success of this experiment corroborated evidence of the existence of the PSD mechanism (Figure 1) [24]. In three other experiments, the decomposition of cells was significantly suppressed due to the inhibition of any of three processes that occurred directly after the impulse shock treatment: transcription from DNA to mRNA, energy-requiring metabolic processes, or lysosomal hydrolytic enzyme activities. Such experiments supported our model [18] by which the PSD mechanism constitutes endergonic, genetically regulated hydrolysis that decomposes a biological polymer into biological monomers. Details are described elsewhere [24].

1.3 Artificial Life Studies

We have also developed a series of simulators of evolution using artificial life, SIVA (simulator for individuals of virtual automata), which provide a basic tool for examining the PSD model. Since 1996, when we constructed SIVA-III [19], a pioneering prototype for an AChem [3, 32] system, we have continued to make enhancements of SIVA [9–11, 20–24, 26], the most current one being the SIVA-T group [11, 24].

FPO

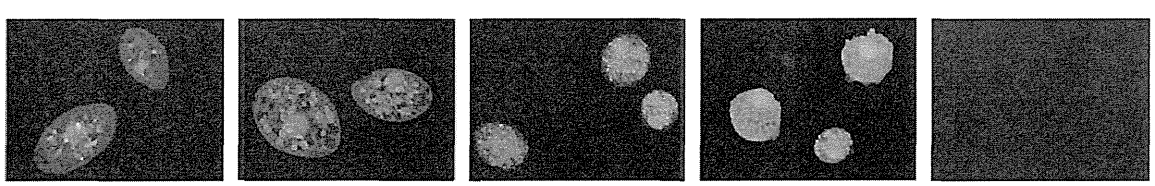

Figure 1. The self-decomposition process in *Tetrahymena* cells induced by impulse heat shock treatment (visualized by acridine orange supravital staining) [24]. *0 hour:* Normal living cells. *1 to 2 hours:* The number of lysosomes (stained orange), an organelle containing hydrolytic enzymes used for self-decomposition, increased. *4 hours:* Lysosomal membranes ruptured and their contents diffused throughout the entire cell. Intracellular hydrolysis turning biological polymers into biological monomers proceeded intensely. *6 hours:* Cell membranes were lysed and cells decomposed into a homogenate state.

SIVA is configured with virtual life individuals (VLIs) installed in a virtual ecosystem in a two-dimensional space. Two different kinds of VLIs are designed for SIVA, based on AChem. One is a VLI of a mortal organism that exerts an altruistic effect through autonomous death accompanied by the PSD mechanism. The other kind is a VLI of an immortal organism having the same structure and functioning as the mortal organism but without autonomous death in the PSD mechanism and thus lacking any altruistic characteristics. Details of the simulator design are described elsewhere [24].

When the two types of VLIs proliferate within the same virtual ecosystem whose environmental conditions are identical throughout the entire ecosystem and are programmed so as to fit both mortal and immortal VLIs, the immortal VLIs prosperously proliferate while, as expected, they exterminate the mortal VLIs, which decrease in number, due to death, during the simulation. This finding well supports the Darwinian principle of survival of the fittest. Actual environmental conditions on Earth, however, are heterogeneous. We therefore designed a virtual environment whose conditions were suitable for VLIs in the initial habitation area, but gradually diverged from the optimal conditions for VLIs. In contradistinction to the above-mentioned results, the immortal VLIs ceased proliferation after occupying the initial areas whose environmental conditions were amenable to their survival, whereas the mortal VLIs succeeded in expanding their habitation area and overwhelmingly surpassed the immortal VLIs [9, 20, 22]. Thus it can be paradoxically stated that a genealogy of living individuals that renounce their self-preservation and self-reproduction prospers to a greater extent than those continuing this pursuit.

The context for such a seemingly contradictory finding is as follows. Mortal VLIs with an altruistic PSD mechanism can endlessly self-reproduce by reusing materials and space restored to the ecosystem due to death and self-decomposition of others and thus cause an increase in the frequency of mutation. Evolutionary adaptation to the environment is accelerated by diversity of species, that is, mutant VLIs evolve one after the other with characteristics that allow them to survive in environmental conditions under which the initial VLIs are unable to survive and thus are able to greatly expand their territory. On the other hand, since immortal VLIs irreversibly fill their habitable area and never reuse it, the available space for existence becomes circumscribed so reproduction becomes increasingly difficult over time. This factor leads to a decrease of emergent mutant VLIs and the blockage of proliferation and evolutionary adaptation. As a result, their inhabitable territory hits a ceiling. We can understand this situation as evidence that autonomous, altruistic self-decomposition accelerates evolutionary adaptation to the environment through the diversification of species.

Moreover, we examined how differences in the degree of altruism affected offspring prosperity using a SIVA simulator endowed with a terrestrial-type finite, heterogeneous environment [24]. In that experiment, we considered the degree of ease for other VLIs to reutilize decomposed parts, which had returned to the environment as a result of self-decomposition, as a hypothetical index of altruism. That is, we designed three different types of mortal VLIs, each of which returned differing types of decomposed parts to environment. The amount of energy required for reutilization by other organisms differed among the three. Namely, the more energy required for reutilization by others, the less altruistic the decomposing organism. We then conducted simulations in which those three types of mortal VLIs and the immortal VLIs proliferated within the same ecosystem. The results showed that the immortal VLIs hit a ceiling at a certain stage, as in the previous experiment, while mortal VLIs with relatively low degrees of altruism on the hypothetical index, hence requiring others to expend a greater amount of energy to reutilize their parts, became extinct. By contrast, mortal VLIs that were decomposed into parts requiring the least amount of energy for reutilization rendered the maximum altruistic contribution to all the other organisms, and thus the whole ecosystem overwhelmingly prospered. The point of such an outcome is that the genealogy of organisms contributing a higher degree of altruism to other organisms allows for greater diversification of the species and accelerates their evolutionary adaptation to the environment. Such findings further support our PSD model and suggest the effectiveness of self-decomposition in the evolution of terrestrial lives.

One of the most critical questions remaining for this hypothesis to stand is a reasonable explanation as to how such an effective gene of altruistic death has emerged in the evolution of terrestrial life. Using our evolutionary model, in which the most primitive form of living individuals is immortal and in which mortal lives emerged by the acquisition of an altruistic death gene as a property highly suitable to the terrestrial environment through the process of evolutionary sophistication [18], we conducted

a preliminary investigation using an artificial ecosystem SIVA-III [19] of our previous design and obtained results that would suggest the robustness of the above hypothesis [10, 22]. Thereafter, we constructed a more sophisticated model for a more detailed investigation making use of an AChem ecosystem SIVA-T05 [24]. The essential questions we sought to answer were as follows: Would an individual mortal organism, overwhelmed by immortal organisms, become extinct, or could such an individual survive and produce offspring? If it survived and produced offspring, what kind of power relationships would be established between such mortal organisms and the immortal ones?

Our findings suggest that a mortal mutant individual, born in an ecosystem where only indigenous immortal organisms exist, cannot repeat self-reproduction steadily and thus becomes extinct in most cases. Nonetheless, some mortal mutant individuals in our study did manage to survive at an extremely small but not negligible rate. Moreover, the offspring of these mortal mutant individuals that survived extended their habitation area, surpassed immortal organisms, and prospered without exception. This article discusses the above findings in detail.

2 Methods

2.1 Design of the SIVA Virtual Environment

In the present study, we again used SIVA-T05 as an evolution simulator. Its construction and functions are the same as those utilized in an earlier report [24]. In short, the virtual environment of SIVA-T05 consists of a lattice of spatial blocks on a two-dimensional plane (Figure 2). Environmental conditions regarding temperature, energy, and four kinds of virtual inorganic biomaterials were independently defined for each spatial block. The initial configuration was identical to that in the previous report [24].

2.2 Structure and Behavior of Artificial Life in SIVA

2.2.1 Structure of a Virtual-Life Individual

As in the earlier report [24], we designed a virtual-life individual (VLI) based on Ohashi's self-reproductive, self-decomposable (SRSD) automaton model (Figure 3), which took von Neumann's self-reproductive automaton model [37] as its prototype. Ohashi's automaton G is described as $G = D + FZ + I_{D+FZ}$, where $D = A + B + C$. Here, automaton A produces automata according to instructions on data tape I (that is, a virtual genome). Automaton B reads and replicates data tape I. Automaton C sets the copy of data tape I replicated by automaton B into new automata produced by automaton A and separates these as automaton D. Automaton FZ, which is a modular subsystem plugged into automaton D, decomposes the whole automaton G into components suitable for re-utilization when automaton G encounters serious environmental conditions in which it is unable to live or has reached the end of its life span. Data tape I_{D+FZ} carries an instruction describing automaton D + FZ. Thus, automaton G, which corresponds to $D + FZ + I_{D+FZ}$, can reproduce an identical automaton G as well as decompose itself.

We designed artificial life based on AChem so as to actualize the above-mentioned logical actions and, as faithfully as possible, to reflect the principles of terrestrial life and its subsequent reproduction (Figure 4). That is, a VLI is constructed from four classes of virtual biomolecules: virtual inorganic biomaterials (VI), virtual organic biomaterials (VO), virtual biological monomers

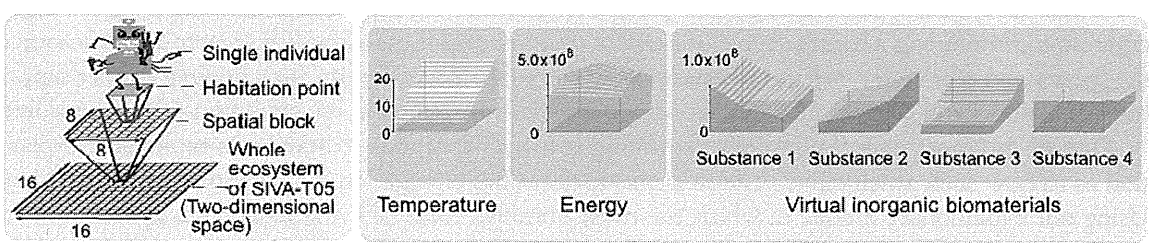

Figure 2. The finite and heterogeneous environmental conditions of the virtual ecosystem SIVA-T05 [24].

FPO

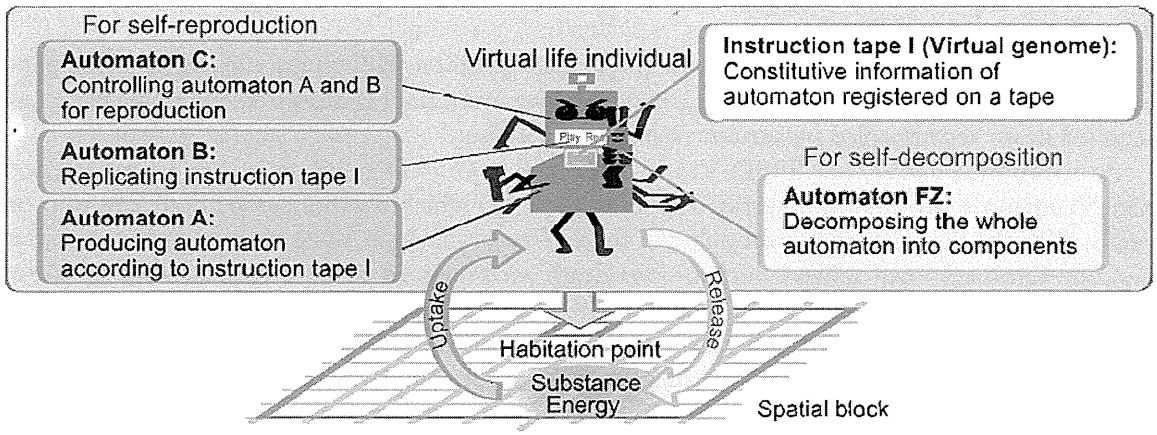

Figure 3. The relationship between life activities of virtual-life individuals (VLIs) and the environment in SIVA-T05 [24].

(VM), and virtual biological polymers (VP). There are four kinds of VI; moreover, any molecules in the latter three classes consist of combinations of the four kinds of VI. A virtual genome in the VP class consists of virtual nucleotides belonging to the VM class. The virtual protein in the VP class is produced according to a sequence of virtual nucleotides that determines the primary sequence of virtual amino acids belonging to the VM class. We developed a SIVA language that actualizes virtual-life activities by recognizing the sequence of the virtual amino acids contained in the virtual protein as coded program sentences and executing therewith. According to given conditions, this SIVA language reproduces, divides, and decomposes a VLI.

2.2.2 Behavior of Virtual-Life Individuals

A VLI executes its life activities by consuming materials and energy from the virtual environment [24]. Activities of each VLI are so designed as to depend on the amount of material and energy available as well as the temperature in the inhabited spatial block. Namely, optimum environmental conditions are defined for each VLI a priori. Activities of a VLI decrease when environmental conditions of the habitation point move away from VLI optimum points. A VLI cannot express its life activities when environmental conditions markedly deviate from the optimum, and, in the case of a mortal organism, it decomposes itself just as it does when it has lived out its life span. Materials and energy released by the decomposition of a VLI are restored to the environment and become utilizable by other individuals within the same space as that occupied by the VLI.

When VLI reproduce, point mutation can occur at a predefined probability during replication of the virtual genome. Mutations may alter the optimum environmental conditions of a VLI. This enables the VLI to live in an environment where it originally could not live. That is to say, evolutionary adaptation to the environment can occur.

FPO

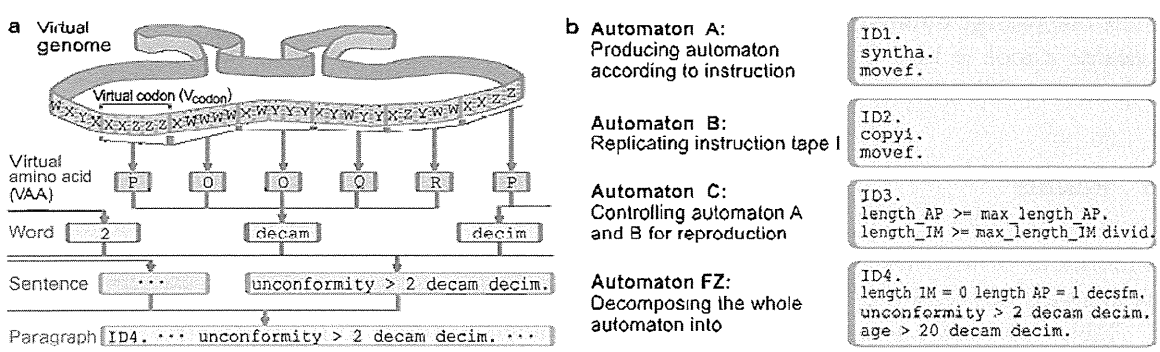

Figure 4. The concept and examples of SIVA language statements that describe the self-reproductive, self-decomposable VLI in SIVA-T05 [24]. (a) Synchesis of virtual protein based on a virtual genome. (b) SIVA language statements describing life activities of automata constituting a SRSD VLI.

2.3 Experimental Setting

We constructed an experimental model to examine our hypothesis [18] on the evolutionary emergence of an altruistic gene using ALife: namely, that primitive immortal organisms through evolution have acquired death accompanied by altruistic self-decomposition.

As mentioned above, our SRSD VLI is described as $G = D + FZ + I_{D+FZ}$. Its prototype is von Neumann's automaton, described as $E = D + I_D$, which reproduces without autonomous death. With the added function module FZ for self-decomposition along with its genetic program I_{FZ}, our automaton can achieve autonomous death accompanied by altruistic self-decomposition. Consequently, mortal organisms are more complex than immortal organisms in terms of structure and function. Von Neumann stated as a matter of principle that "when an automaton performs certain operations, they must be expected to be of a lower degree of complication than the automaton itself"; furthermore, he described living organisms as follows [37]: "They produce new organisms with no decrease in complexity. In addition, there are long periods of evolution during which the complexity is even increasing." Our self-decomposable mortal automaton, having greater complexity, achieves prosperity of its offspring exceeding that of its immortal prototype. Consequently, we hypothesized that mortal organisms with altruistic self-decomposition emerge evolutionarily from immortal organisms [18, 22].

We constructed our experimental simulation model using SIVA configured with a terrestrial-type finite, heterogeneous environment. First, we designed an immortal organism as a precursor at an evolutionary stage just prior to its becoming a mortal organism, and configured a virtual ecosystem inhabited by that precursor organism as its only indigenous species. Then we considered what might become of a mortal individual with altruistic self-decomposition that had emerged evolutionarily from an indigenous immortal organism through mutation. As shown in Figures 3 and 4, the mortal VLIs consist of automata A, B, C, and FZ, each of which is a virtual protein with a specific function, as well as a data tape I_{D+FZ}, that is, a virtual genome that stores the data for each automaton. Automaton FZ, which has decomposed VLI itself, was activated whenever either of the following conditions was determined to be true: (1) the VLI encountered an environment incompatible with its survival, or (2) the VLI's life span had ended. For immortal VLIs, therefore, we assumed such conditions to be false so as not to make FZ execute self-decomposition. If this mechanism became the target of a mutation that canceled the "false" setting, it would correctly determine the above conditions to be true. Consequently, the mutant VLI could activate FZ and execute its own self-decomposition, resulting in the evolutionary emergence of a mortal organism with altruistic self-decomposition. We seeded an immortal VLI possessing this precursor of a genetic program for death at the very center habitation point of an ecosystem whose environmental conditions were deemed most suitable for a VLI.

The mutation rate was determined as follows. Existing terrestrial lives tend to have a higher mutation rate, as the length of their genome is shorter. For example, an organism with a genome of 10^4 molecules has a mutation rate 10^{-4}. Since the virtual genomes of VLIs in the present simulation consisted of 1,275 VM molecules, we used three mutation rates: 0.005, 0.002, and 0.001.

For each of the three mutation rates, we conducted 200 to 800 simulations of 800 passage durations each and observed changes in size of habitation area, number of VLIs, and frequency of mutation. Here one passage duration corresponded to 5 time counts (TCs, the unit of virtual time in SIVA-T05), because it took at least 5 TCs for a newborn individual to reproduce itself in our current simulation experiments. We have used the passage duration as the time unit in this report.

3 Results

Simulations of whether mortal VLIs emerging from immortal VLIs through mutation survived and proliferated obtained the following results.

Table 1 shows the proportions of the simulations in which mortal VLIs emerged and then survived at each mutation rate. Not so many mortal mutants emerged evolutionarily within the passage duration of 800, and, even when emerging, most of them were surpassed by native immortal VLIs and did not survive. The survival rates of emerging mortal mutants, however, were not negligible: 3.5%, 1.4%, and

Table 1. Proportions of the evolutionary emergence and survival of mortal virtual-life individuals.

Mutation rate	Total number of simulations	Proportion of emergence (number of simulations)	Proportion of survival (number of simulations)	Survival proportion of simulations with emergence
0.005	200	29% (58)	3.5% (7)	12%
0.002	500	11% (56)	1.4% (7)	13%
0.001	800	5.3% (42)	0.25% (2)	4.8%

0.25%, respectively, of the total number of simulations at mutation rates of 0.005, 0.002, and 0.001. Namely, the mortal mutants and their offspring that evolutionarily acquired altruistic self-decomposition were mostly but not altogether exterminated, with some surviving in extremely low proportions.

It was noteworthy that once the emerging mortal mutants survived and left offspring, these invariably surpassed immortal VLIs and increasingly proliferated as the passage duration became longer. Figure 5 shows changes in habitation area, number of VLIs, and frequency of mutation in a typical example for each of the three mutation rates, and indicates that the numbers of individuals and the frequency of mutation of mortal VLIs were quite low as they began to emerge, but, as their activity gradually increased, they began to surpass immortal VLIs between passage durations of 300 and 400, and afterwards proliferated exponentially.

4 Discussion

4.1 Emergence and Prosperity of Mortal Organisms

We carried out an evolutionary simulation experiment using our artificial ecosystem SIVA-T05, modeled for a finite, heterogeneous terrestrial environment and arranged in a biomolecular hierarchy. When a mortal mutant individual endowed with an evolutionarily acquired genetic program for death was born in a place in which immortal organisms already existed as indigenous ones, although

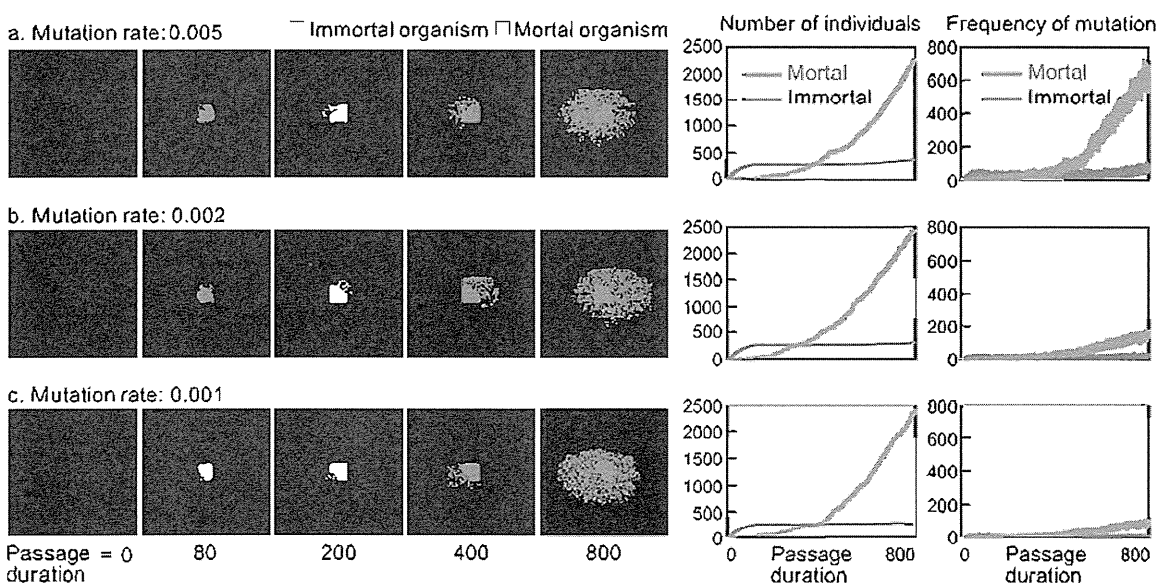

Figure 5. Successive changes in the distribution of individuals, the number of individuals, and the frequency of mutation of mortal and immortal VLIs when mortal VLIs emerged evolutionarily from immortal VLIs through mutation in the ecosystem where only immortal VLIs existed: (a) mutation rate 0.005; (b) mutation rate 0.002; (c) mutation rate 0.001. The mortal VLIs, which emerged and survived at a very low ratio, clearly surpassed immortal VLIs and became prosperous with adaptive divergence under various environmental conditions.

such mortal individuals had difficulty in surviving, yet they did survive and produced offspring, albeit at a very low reproductive rate. We also showed that, once these living individuals survived, they invariably prospered and surpassed existing immortal organisms.

Is it possible to apply such a finding to the actual evolutionary history of the terrestrial ecosystem? For example, since the evolution and prosperity of mortal organisms were only observed twice out of eight hundred simulations with a mutation rate of 0.001, such a result might be deemed merely an extremely rare phenomenon. However, in consideration of the enormously long evolutionary period of 3.8 billion years since most ancestors of life emerged, the boundless expanse of the terrestrial environment relative to a unicellular organism as minute as a few microns, for which even a cubic meter of water environment would be greatly expansive, and the immeasurable diversity and heterogeneity of matter and energy, we suggest that evolution from immortal to mortal life might well occur even if the probability might be lower than what we employed in the simulations.

4.2 Background to the Superiority of Mortal Organisms

As shown in our research, including the current experiment, the superiority of mortal organisms to immortal organisms pertains to the following background. Immortal organisms dominate space and materials, once secured, while the volume of resources in the ecosystem to sustain life activities monotonically decreases. With less chance of reproduction in association with a decrease of resources, the chances for mutation and evolutionary adaptation are reduced. By contrast, mortal organisms through self-decomposition release space and return their parts to the environment for other organisms to reutilize. As a result, accumulated mutations through the continuous alternation of generations accelerate evolutionary adaptation to the environment.

Death is the non-reversible termination of two definitive attributes of living individuals, namely, self-preservation and self-reproduction. In terrestrial lives, these attributes are associated with autolysis, which we have modeled as programmed death accompanied by altruistic self-decomposition, that is, the restoration of biomaterials and habitation space to the environment. In terrestrial lives, moreover, death is triggered not only by external forces such as predation, injury, or infection, but also by overwhelming environmental unconformity and the normal life span of that species. Consequently, death is essentially inevitable for terrestrial lives.

From the viewpoint of the individual-centric umwelt[1] considering the life principles of self-preservation and self-reproduction, such death of a terrestrial life form can be understood as the last defect of life, which should be essentially flawless, and as the epitome of the incompleteness of life, which could be overcome through evolution. Nonetheless, in our previous evolutionary simulation studies based on the ecosystem-dominant umwelt model, we found that living individuals endowed with a mortal genetic program that includes altruistic self-decomposition prospered and surpassed flawless living individuals with perfect self-preservation and self-reproduction in a heterogeneous, complex, terrestrial-type virtual environment.

The current experiment revealed that offspring of indigenous immortal organisms prospered more significantly than did their parents because of the autonomous, altruistic mortal genetic program newly installed in the immortal organisms that converted them into mortal organisms; that is, they evolutionarily acquired a paradoxical survival strategy. This finding encourages us to create a model for the acquisition of autonomous, altruistic death as the fruit of evolution.

Independent of the studies that we have undertaken since 1987 [9–11, 18–26], Peter M. Todd implemented artificial death in his ALife system [33, 34], and those experiments supported the recognition shared with us that death affords another entity its space in which to exist, and that death, accordingly, is essential throughout the ongoing evolutionary process. Nevertheless, the model of death constructed by Todd differs from ours in two obvious respects. First, death in Todd's model affords no process by which the organism might decompose itself into constituent parts for the efficient and collective reutilization of other organisms, which is an essential feature of our model. Second, the

1 The concept of *Umwelt* as proposed by Jakob von Uexküll [38].